J Mater Sci (2012) 47:739–745
DOI 10.1007/s10853-011-5848-2

Enhancement of thermal stability of TiO_2 nanowires embedded in anodic aluminum oxide template

Xiaoliang Wang

Received: 20 May 2011 / Accepted: 3 August 2011 / Published online: 23 August 2011

Abstract Titania (TiO_2) nanowires with diameters of 20, 50, and 80 nm were successfully synthesized via the template-assistant method. The TiO_2 nanowires embedded in anodic aluminum oxide template have extremely high crystallization and anatase-to-rutile phase transition temperatures than that of the free-state TiO_2 powders, and the thermal stability of embedded TiO_2 nanowires depends on the diameter of the templates. The growth and nucleation activation energy of rutile in 20 nm nanowires are determined to be $E_g = 2.8 \pm 0.2$ eV and $E_n = 2.7 \pm 0.2$ eV, respectively, much higher than that of the free-state TiO_2 powders with $E_g = 1.6 \pm 0.2$ eV and $E_n = 1.9 \pm 0.2$ eV. The pressure induced by the difference of thermal expansion coefficient between the TiO_2 and aluminum oxide acts as an effective barrier that prevents phase transition, resulting in the enhancement of the TiO_2 structural stability.

Introduction

One-dimensional inorganic nanostructures exhibit a wide range of electrical and optical properties due to the size-dependent properties [1]. Titania (TiO_2) has been widely studied because of its unique optical and chemical properties in catalysis [2], photocatalysis [3], sensitivity to humidity and gas [4, 5], nonlinear optics [6], photoluminescence [7], and so on. Naturally, TiO_2 has three different crystallographic forms: brookite, anatase, and rutile, and the properties of TiO_2 are very sensitive to its crystal structure [8, 9]. For example, Anatase has been found to be much more active than that of the rutile phase in photocatalysis [8]. While at ambient pressure and temperature, the rutile phase is more thermodynamically stable than that of the anatase phase, which is kinetically stable phase at relatively low temperature [10]. Several methods, including the preparation TiO_2-based nanocomposites (TiO_2/alumina, TiO_2/silica) and surface impurities, have been reported to increase the stability of the anatase structure [11–13]. However, most of the reports deal with the preparation of the composite using surfactant, and it is difficult to eliminate the organic agent from the sample [14]. Therefore, a direct preparation of high thermal stability titania with surfactant-free method is of particular interest.

Previous studies revealed that the role of confinement from the interface and the difference of thermal expansion between the core and shell are significant in the phase stability of materials [15, 16]. For instance, Wang et al. [15] observed the large superheating of the α-Sn phase encapsulated in SnO_2 nanotube with the diameter of 10 nm. Mei et al. [16] studied the pressure effect of the superheating of the Al nanoparticles encapsulated in Al_2O_3 shell and observed 7–15 K beyond the bulk equilibrium melting point of Al. However, the crystallization and structural transition of TiO_2 nanowires in confined space are still poor understood. Herein, the thermodynamics and kinetics studies of the TiO_2 nanowires embedded in Anodic Aluminum Oxide Template (AAT) are reported. The embedded nanowires have extremely high crystallization and anatase-to-rutile phase transition temperatures and the thermal stability of TiO_2 shows obvious size-dependent property.

X. Wang (✉)
State Key Laboratory of Metastable Materials Science and Technology, Yanshan University, 066004 Qinhuangdao, People's Republic of China
e-mail: wxlsr66@gmail.com

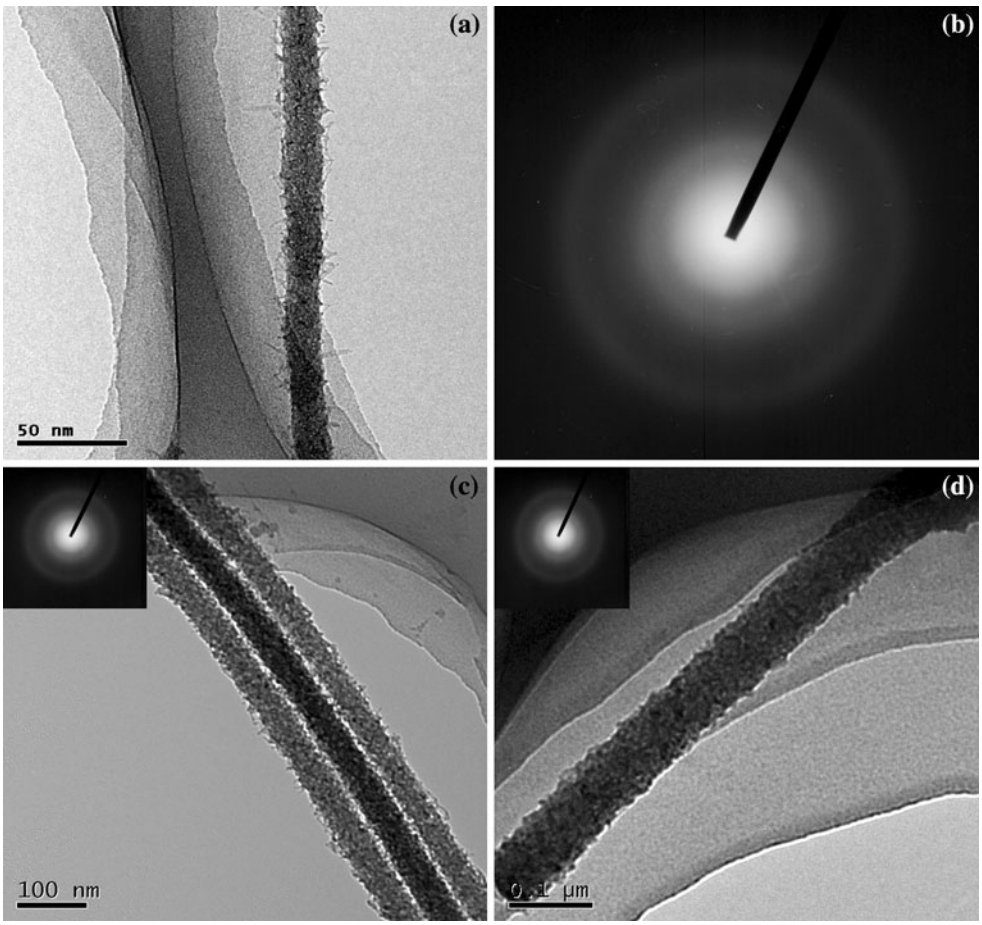

Fig. 1 Typical TEM image of as-prepared nanowires with diameters of **a** 20, **c** 50, and **d** 80 nm, **b** the SAED patterns of the nanowires

Experimental

The AAT were prepared by a two-step anodization process as described by Masuda and Fukuda [17]. Typically, the template with the pore diameters of 20 nm were prepared by anodized aluminum foil in 0.3 M sulfuric acid with the potentials of 25 V at 5 °C. The templates with the pores of 50 nm in diameters were prepared by anodized in 0.3 M oxalic acid with the potentials of 40 V. The 80 nm AAT were prepared by anodized in 0.3 M oxalic acid with the potentials of 40 V and then etching in the 5 wt% phosphoric acid for about 40 min [18]. TiO_2 nanowires were prepared using a sol–gel process with AAT. In brief, the AAT were immersed in 10 mL of tetrabutyl titanate at room temperature for 30 min, then the wet AAT were hydrolyzed with addition few droplets of 0.1 M HCl aqueous solution and dried it in an oven at 50 °C for 12 h. TiO_2 powders were obtained by hydrolyzing tetrabutyl titanate with 0.1 M HCl aqueous solution and then dried in an oven at 50 °C for 12 h. The microstructures of the samples were characterized by employing the XRD measurements. For TEM and selected-area electron diffraction observations, the AAT was fully dissolved using NaOH (0.5 M) solution.

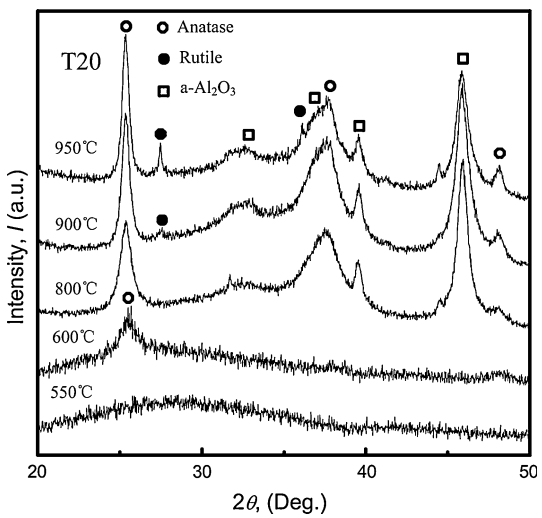

Fig. 2 The XRD patterns of the T20 in AAT after annealing at different temperatures for 1 h

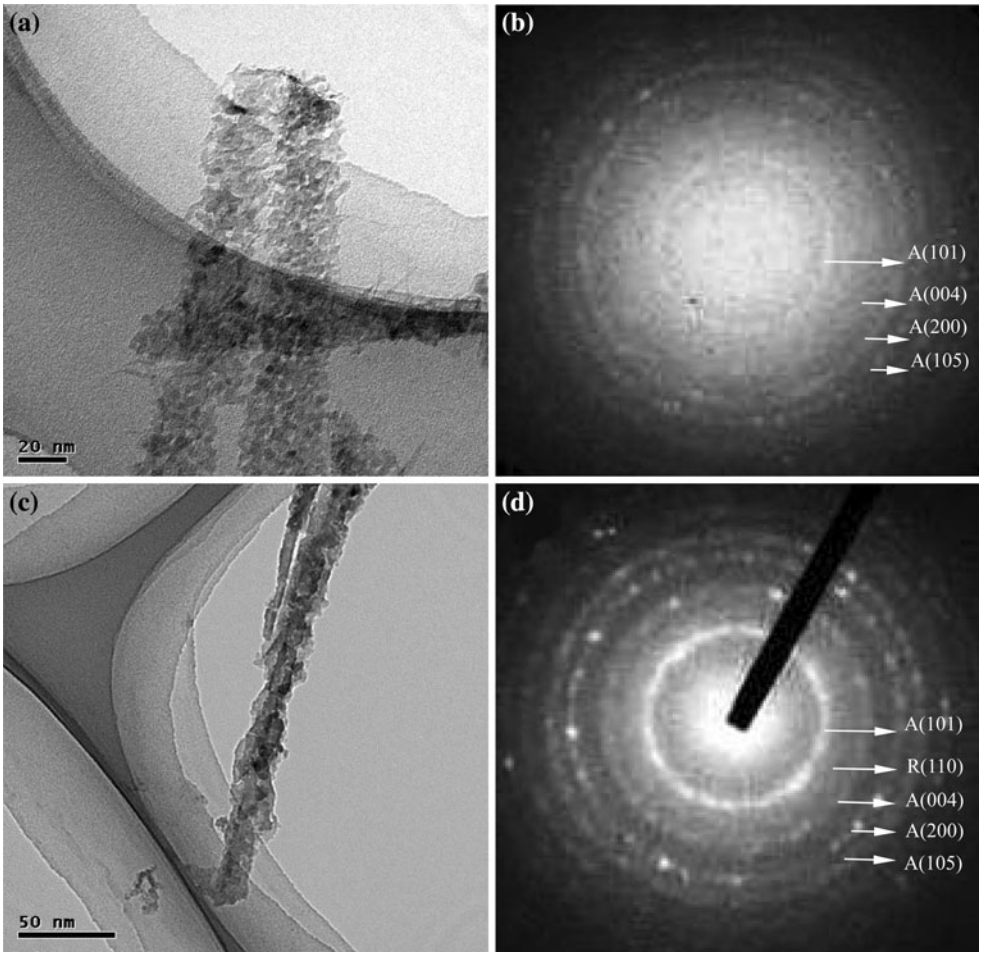

Fig. 3 **a**, **c** Typical TEM images of the T20 after annealing at 600 and 900 °C for 1 h, respectively. **b**, **d** The corresponding SAED patterns

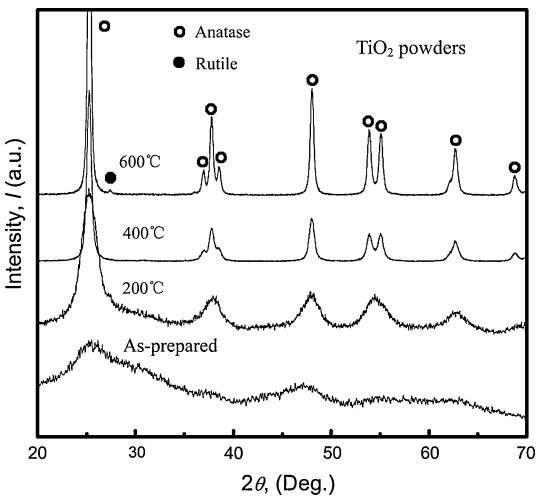

Fig. 4 The XRD patterns of the free-state TiO_2 powders after annealing at different temperatures for 1 h

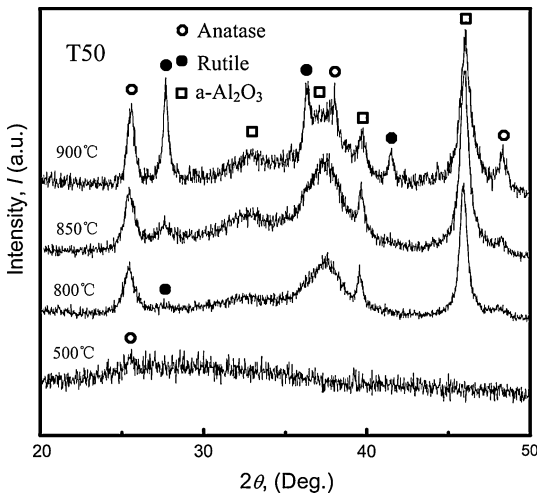

Fig. 5 The XRD patterns of the T50 in AAT after annealing at different temperatures for 1 h

Results and discussion

The typical TEM images of the synthesized TiO_2 nanowires with the average diameters of 20, 50, and 80 nm (denoted as T20, T50, and T80) are showed in Fig. 1. The selected-area electron diffraction patterns of the as-prepared samples show amorphous structural character (see Fig. 1b).

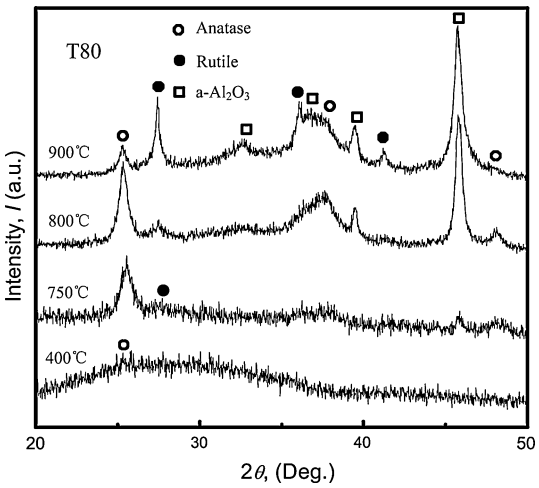

Fig. 6 The XRD patterns of the T80 in AAT after annealing at different temperatures for 1 h

Figure 2 shows the XRD patterns of annealed T20 embedded in AAT at different temperatures for 1 h. The crystallization of the T20 occurs at about 600 °C. With the calcination temperature increased to 800 °C, α-Al_2O_3 crystallize from AAT appears, but the T20 still shows anatase structure. Increasing the calcination temperature to 900 °C, we find rutile is obtained. Figure 3 shows the bright field images and the corresponding diffraction patterns for T20 annealed at 600 and 900 °C for 1 h, respectively. The results confirmed that the crystallization temperature and structure transition temperature of T20 sample are 600 and 900 °C, respectively, which are in agreement with the XRD results. In order to study the confinement effect of AAT on the phase transition behavior, the free-state TiO_2 powders at various annealing temperature were determined by XRD (see Fig. 4). It can be seen that the free-state TiO_2 powders crystallize at 200 °C and structural transition starts at about 600 °C, which are much lower than that of the embedded TiO_2 nanowires.

The above results suggest that inhibition of crystallization and structural transition may be caused by the confinement of the AAT [17, 18]. To further explore the effect of confinement on the structural stability of TiO_2

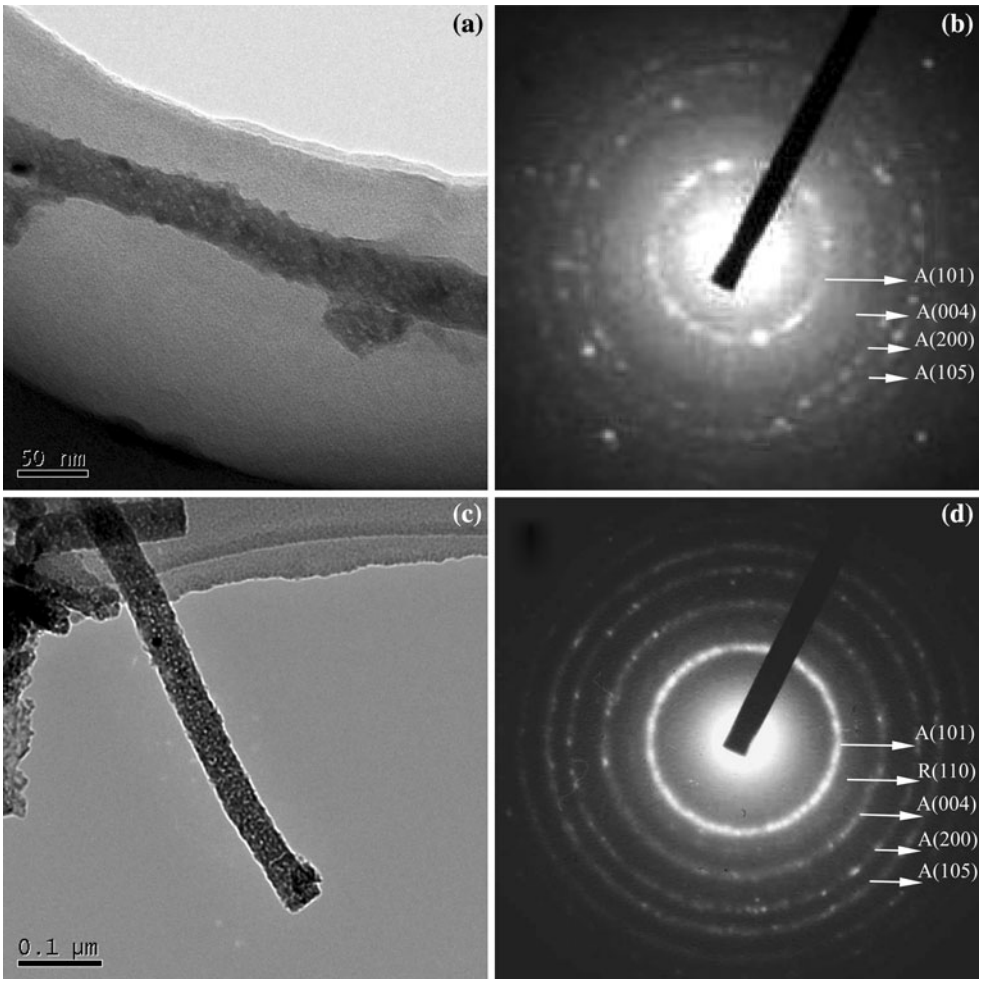

Fig. 7 **a**, **c** Typical TEM images of the T50 after annealing at 500 and 800 °C for 1 h, respectively. **b**, **d** The corresponding SAED patterns

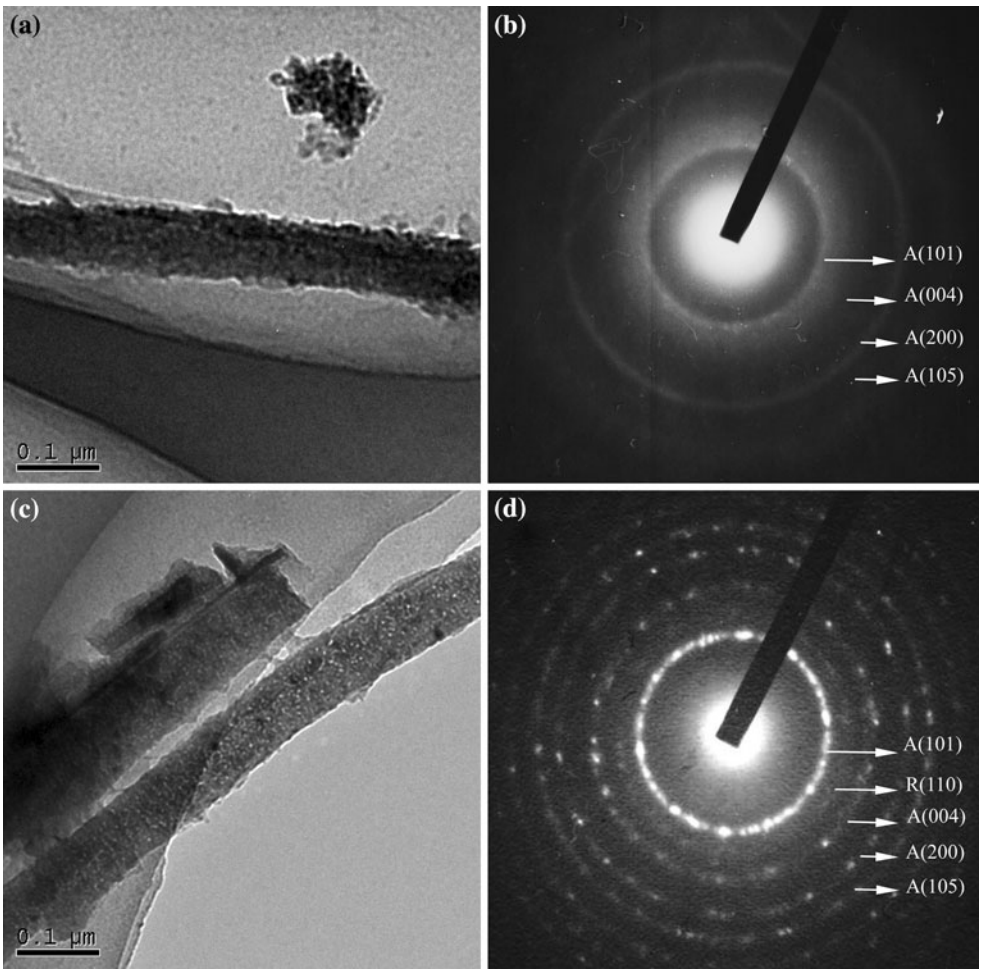

Fig. 8 **a**, **c** Typical TEM images of the T80 after annealing at 400 and 750 °C for 1 h, respectively. **b**, **d** The corresponding SAED patterns

nanowires, T50 and T80 nanowire arrays embedded in AAT are annealed at different temperatures. It can be seen that for T50 sample with the diameter of 50 nm, the characterized peaks corresponding to the anatase (101) plane and rutile (110) plane appear at 500 and 800 °C, respectively (see Fig. 5). When the diameter of the TiO_2 nanowires increases to 80 nm, the crystallization and phase transition temperatures decrease to 400 and 750 °C, respectively (see Fig. 6). Those are directly confirmed by TEM studies (see Figs. 7, 8). The results reveal a strong size dependence of the thermal stability of TiO_2 nanowires embedded in the AAT.

A detailed study of the nucleation and growth kinetics of nanocrystalline anatase to rutile was performed by in situ X-ray diffraction techniques. Figure 9a, c present the annealing time dependence of the mean size d of the rutile of T20 and free-state TiO_2 at different temperatures. The size of the rutile shows an exponent-shaped increase with annealing time t. It is quite clear that the time needed to reach the saturation-state growth rate (i.e., $\partial d/\partial t = 0$), which is defined as the saturation time constant t_E, varies with the annealing temperature. To determine the t_E, the experimental data shown in Fig. 9 were fitted by:

$$d(t) = d_s - (d_s - d_0)A_0 \exp\left(-\frac{t}{t_E}\right) \quad (1)$$

where d_0 and d_s are the initial and growth saturation sizes of the rutile nanoparticles, respectively.

The saturation time constant t_E decreases with increasing the annealing temperature T (see Fig. 9a), indicating that the growth of the rutile is a thermally activated process. Assuming the saturation rate t_E^{-1} has an Arrhenius temperature dependence, we have

$$t_E^{-1} = t_{E.0}^{-1} \exp\left(-\frac{E_g}{k_B T}\right) \quad (2)$$

where E_g is the growth activation energy, $t_{E.0}$ is the pre-exponential factor, and k_B is the Boltzmann's constant. An Arrhenius plot shown in Fig. 9b yields a growth activation energy $E_g = 2.8 \pm 0.2$ eV for the rutile in the TiO_2 nanowires.

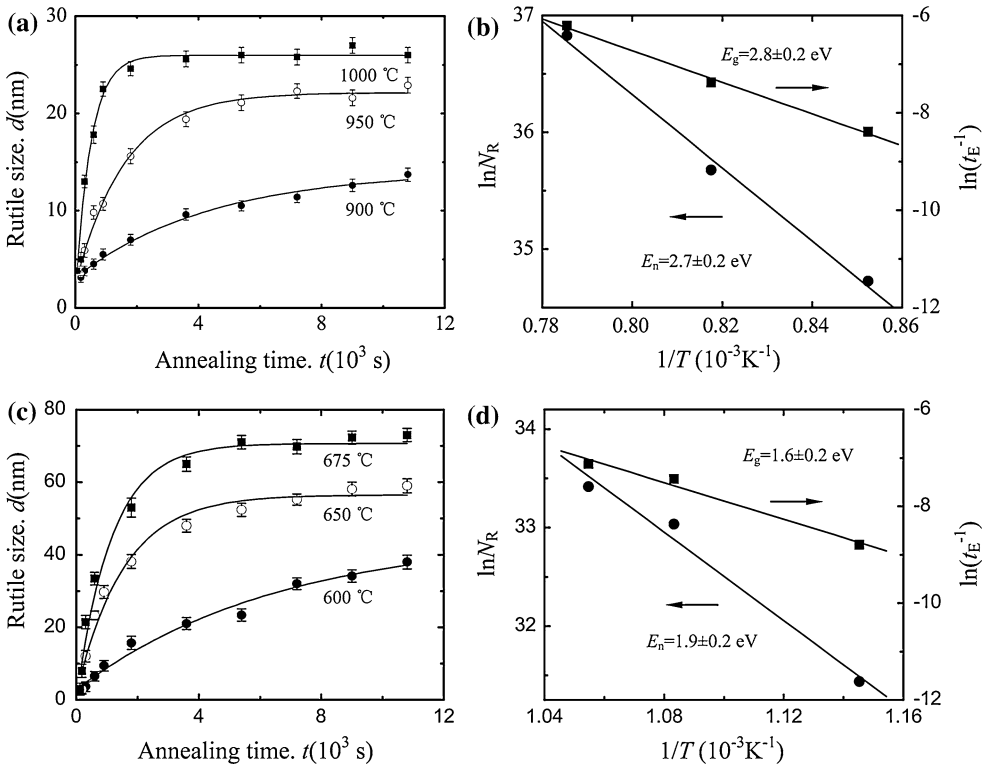

Fig. 9 **a**, **c** Annealing time dependence of the size of the rutile in the T20 and free-state powders at different temperatures. **b**, **d** Annealing temperature variations of the nucleation rate N_R and the growth saturation rate t_E^{-1} for rutile in the T20 and free-state powders, respectively. The growth and nucleation activation energy are yielded according to Eqs. 2 and 4, respectively

No obvious increase in the size of the rutile is observed after annealing in the temperature range from 900–1000 °C for 1 min (see Fig. 9a). Therefore, the increase of the volume fraction in the annealing temperature range depends dominantly on the nucleation of the rutile. This allows the nucleation process of the rutile nanoparticles to be investigated independently. The nucleation rate N_R of the rutile at the annealing temperatures (for 1 min) is determined by employing XRD measurements according to

$$N_R = \frac{\Delta V}{V_0 \cdot \Delta t} \tag{3}$$

where V_0 is the volume of the rutile at $t = 1$ min, $\Delta V = V_{T(t)} - V_R, V_{T(t)}$and V_R are the volume fraction of the rutile at annealing temperature T for 1 min and at room temperature (here, $V_R = 0$), respectively; Δt is the time for the variation of the volume fraction ΔV of the rutile.

The nucleation rate N_R of the rutile determined by the XRD studies increases with increasing annealing temperature (see Fig. 9), indicating that the nucleation of the rutile is also a thermally activated process. According to the Arrhenius temperature dependence [19], we have, for $t = 1$ min,

$$N_R = N_{R,0} \exp\left(-\frac{E_n}{k_B T}\right) \tag{4}$$

where E_n is the activation energy for the formation of the rutile, $N_{R,0}$ is the preexponential factor. The Arrhenius plots shown in Fig. 9b yield a similar nucleation activation energy $E_n = 2.7 \pm 0.2$ eV.

Using the similar methods, the growth and nucleation activation energy for rutile in free-state TiO_2 powders in the temperature range of 600–700 °C are yielded to be $E_g = 1.6 \pm 0.2$ eV and $E_n = 1.9 \pm 0.2$ eV, respectively (see Fig. 9c, d). This value can be compared with the nucleation activation energy $E = 185.1$ kJ/mol ($E_n = 1.92$ eV) reported by Zhang et al. [20], which is much smaller than that of the confined-state TiO_2 nanowires ($E_n = 2.7$ eV). The results indicate that it is much more difficult to nucleate and grow for the rutile phase confined in the channels of the AAT than free-state powders.

We want to point out here that the restriction by the channels of alumina membrane may inhibit the structural change, greatly increase the thermal stability of TiO_2 nanowires. The extremely high thermal stability of anatase encapsulated in the AAT is attributed to the pressure induced by the difference of thermal expansion coefficient between Al_2O_3 (7.5×10^{-6}/K) [21] and TiO_2 (8.5×10^{-6}/K) [22] upon heating. Al_2O_3 is the stiffest and strongest oxide ceramics with a shear modulus of about 150 GPa [23]. Supposing the AAT is constructed by a bundle of hollow cylindrical and the column diameters are uniform, the overpressure on the TiO_2 core encapsulated by the Al_2O_3 shell can be calculated using the modifying shell model [21]:

$$P = \frac{2\mu_s \Delta T \cdot \Delta\alpha}{\frac{2\mu_s}{3K_c}\frac{1-\nu_c}{1-2\nu_c} + \frac{b^2+\frac{1-3\nu_s}{1-\nu_s}a^2}{b^2-a^2}} \tag{5}$$

where μ_s is the shear modulus of the shell, K_c is the bulk modulus of the core, $v_c$and v_s are the Poisson's ratio, a and b are the radius of the core and shell, respectively, ΔT is the temperature difference, and $\Delta\alpha$ is the thermal expansion coefficient difference between TiO_2 and Al_2O_3. By parameters as previously reported, we calculated the pressure as a function of the relative shell/core ratio (a/b) and the temperature difference (ΔT). For sample T20, T50, and T80, the pressure derived from the shell model are about 0.13, 0.10, and 0.05 GPa at 900, 800, and 750 °C, respectively.

In anatase TiO_2 nanoparticles, the excess pressure compresses the particle, resulting in a contraction in the Ti–O bond [24], and hence a stronger binding between Ti an O atoms. As a result, more thermal energy is needed to break and rearrange bonds to nucleate rutile at anatase surfaces. This causes an increase in the activation energy that can be assumed to be proportional to the excess pressure [20], which can be expressed as the following:

$$E_n = E_n(\infty) + cP + E_0 \quad (6)$$

where $E_n(\infty)$ is the activation energy for nucleation in bulk anatase, E_0 is the affinity energy of Ti–O–Al bond, P is the excess pressure, and c is proportional coefficient. A linear relationship exists between the nucleation activation energy and the pressure. Assuming E_0=0, gave $c = 6.15$ eV/GPa, then E_n(T50) $= 2.5 \pm 0.2$ eV, and E_n(T80) $= 2.2 \pm 0.2$ eV, respectively. The increase in nucleation activation energy confirmed the retarding effect of AAT on the anatase-to-rutile phase transition.

Conclusion

In summary, we successfully synthesized TiO_2 nanowires by simple methods with different diameters. The embedded nanowires have extremely high crystallization and anatase-to-rutile phase transition temperatures and the thermal stability of titania depends on the diameter of the AAT. The growth and nucleation activation energy of rutile in the embedded nanowires are much higher than the free-state titania powders. The pressure induced by the difference of thermal expansion coefficient between the titania and alumina act as an effective barrier that prevents phase transition, resulting in enhancement of the TiO_2 structural stability. This study could be of importance not only in fundamental interest, but also in the structural design, thermal stability of future nanodevices.

References

1. Xia Y, Yang P, Sun Y, Wu Y, Mayers B, Gates B, Yin Y, Kim F, Yan H (2003) Adv Mater 15:353
2. Bradford MCJ, Vannice MA (1996) Appl Catal A 142:73
3. Thompson TL, Yates JT (2006) Chem Rev 106:4428
4. Yeh YC, Tseng TT, Chang DA (1989) J Am Ceram Soc 2:1472
5. Ketrom L (1989) Am Ceram Soc Bull 68:860
6. O'Regan B, Gratzel M (1991) Nature 353:737
7. Liu YJ, Claus RO (1997) J Am Chem Soc 119:5273
8. Zhu JF, Zheng W, He B, Zhang JL, Anpo M (2004) J Mol Catal A 216:35
9. Gerscher H, Heller A (1991) J Phys Chem 95:5261
10. Ovenstone J, Yanagisawa K (1999) Chem Mater 11:2770
11. Wang Z, Deng X (2007) Mater Sci Eng B 140:109
12. Gao X, Wachs Catal IE (1999) Today 51:233
13. Chen B, Zhang H, Gilbert B, Banfield JF (2007) Phys Rev Lett 98:106103
14. Aronson BJ, Blanford CF, Stein A (1997) Chem Mater 9:2842
15. Wang B, Ouyang G, Yang YH, Yang GW (2007) Appl Phys Lett 90:121905
16. Mei QS, Wang SC, Cong HT, Jin ZH, Lu K (2005) Acta Mater 53:1059
17. Wang Y, Ye C, Wang G, Zhang L, Liu Y, Zhao Z (2003) Appl Phys Lett 82:4253
18. Wang XW, Fei GT, Wu B, Chen L, Chu ZQ (2006) Phys Lett A 359:220
19. Starink MJ (2003) Thermochim Acta 404:163
20. Zhang H, Banfield JF (2005) Chem Mater 17:3421
21. Spaepen F, Turnbull D (1979) Scr Metall 13:149
22. Jagtap N, Bhagwat M, Awati P, Ramaswamy V (2005) Thermochem Acta 427:37
23. Shackelford JF, Alexander W (2001) CRC materials science and engineering handbook, 3rd edn. CRC, Boca Raton
24. Chen LX, Rajh T, Jager W, Nedeljkovic J, Thurnauer MC (1999) J Synchrotron Rad 6:445